J|A|C|S
ARTICLES
Published on Web 08/19/2006

Cruciforms as Functional Fluorophores: Response to Protons and Selected Metal Ions

Anthony J. Zucchero, James N. Wilson, and Uwe H. F. Bunz*

Contribution from the School of Chemistry and Biochemistry, Georgia Institute of Technology, 770 State Street, Atlanta, Georgia 30332

Received February 15, 2006; E-mail: uwe.bunz@chemistry.gatech.edu

Abstract: The photophysics of dialkylamino- and/or pyridine-containing functional chromophores, 1,4-distyryl-2,5-bis(ethynylaryl)benzenes (cruciforms) was investigated; their fluorescence quantum yields and emissive lifetimes were determined. Depending upon their substituents, the frontier molecular orbitals (FMOs) of these cruciforms are either congruent, i.e., HOMO and LUMO occupy the same real space, or disjoint, i.e., the HOMO is located on one branch of the cruciform while the LUMO is located on the second one. Donor−acceptor substitution leads to a disjoint FMO pattern, while the parent 1,4-distyryl-2,5-bis(phenylethynyl)-benzene shows congruent FMOs. The photophysics of the cruciforms was investigated upon addition of either an excess of trifluoroacetic acid or an excess of selected metal (Mg^{2+}, Ca^{2+}, Mn^{2+}, Zn^{2+}) trifluoromethanesulfonate salts. Addition of either metal ions or protons led to analogous but not identical changes in the spectroscopic properties of the investigated cruciforms. The collected data suggest that the metals bind preferentially at the aniline nitrogen and not at the electron-rich arene. The spatially separated FMOs permit the independent manipulation of the HOMO and the LUMO of such cruciforms. If the branches contain metal-complexing moieties, metal binding leads to either a hypsochromic or a bathochromic shift in emission via interaction of the metal cations with either the HOMO or the LUMO.

Introduction

Functional chromophores contain embedded recognition elements as integral parts of their π-system. Such chromophores are innately qualified to serve as active elements in sensors or sensor arrays and in advanced materials applications. *Functional* chromophores are different from *functionalized* chromophores, where recognition elements are merely appendages affixed to a fluorescent core. Functional chromophores undergo analyte-induced shifts in absorption and emission; the binding modulates electronic properties due to the interweaving of π-system and recognition element. Prominent examples are Zn−ESIPT sensors and related phores,[1] bipyridine-containing conjugated polymers,[2] tetraethynylethenes (TEEs) and diethynylethenes (DEEs),[3] and oligophenyleneethynylene-embedded 2,6-bis(1,9-methylbenzimidazolyl)pyridines.[4] Whenever basic nitrogens or phenolates are an integral part of a dye, functional chromophores result. Pyridines, bipyridines, and terpyridines as well as aromatic dialkylamines, phenolates, and phosphines, inter alia, are good candidates to render a chromophore "functional". Embedded bases can be either strongly electron accepting, such as pyridines, or strongly electron donating, such as dialkylanilines, permitting the rational design of functional chromophores with modular photophysical responses. If donor and acceptor units are spatially separated, it will be possible to address HOMO and LUMO independently by Lewis acids or metal cations. A chromophore system will result that naturally displays a two stage response or differential binding to an electron deficient analyte. Cruciforms **1**−**7** are functional chromophores, with incorporated basic nitrogens; they should show potential in the fabrication of functional sensor arrays for metal ions.[5]

To fully understand and appreciate the subtleties and issues associated with the sensory response of these cruciform chromophores, we report the steady-state photophysics and the emissive lifetimes of **1**−**7** and their response to the addition of protons and the triflates of Mg^{2+}, Ca^{2+}, Mn^{2+}, and Zn^{2+}. We selected these metal cations as they are all biologically active, +2 charged ions of similar size. Large shifts in absorption,

(1) (a) Henary, M. M.; Wu, Y. G.; Fahrni, C. J. *Chem.—Eur. J.* **2004**, *10*, 3015−3025. (b) Pond, S. J. K.; Tsutsumi, O.; Rumi, M.; Kwon, O.; Zojer, E.; Bredas, J. L.; Marder, S. R.; Perry, J. W. *J. Am. Chem. Soc.* **2004**, *126*, 9291−9306.

(2) Wang, B.; Wasielewski, M. R. *J. Am. Chem. Soc.* **1997**, *119*, 12−21. Bangcuyo, C. G.; Rampey-Vaughn, M. E.; Quan, L. T.; Angel, S. M.; Smith, M. D.; Bunz, U. H. F. *Macromolecules* **2002**, *35*, 1563−1568. (c) Pautzsch, T.; Klemm, E. *Macromolecules* **2002**, *35*, 1569−1575.

(3) Gobbi, L.; Seiler, P.; Diederich, F. *Angew. Chem., Int. Ed.* **1999**, *38*, 674−678. (b) Diederich, F. *Chem. Commun.* **2001**, 219−227. (c) Tykwinski, R. R.; Gubler, U.; Martin, R. E.; Diederich, F.; Bosshard, C.; Gunter, P. *J. Phys. Chem. B* **1998**, *102*, 4451−4465. (d) Tykwinski, R. R.; Schreiber, M.; Carlon, R. P.; Diederich, F.; Gramlich, V. *Helv. Chim Acta* **1996**, *79*, 2249−2281. (e) Hilger, A.; Gisselbrecht, J. P.; Tykwinski, R.; Boudon, C.; Schreiber, M.; Martin, R.; Lüthi, H. P.; Gross, M.; Diederich, F. *J. Am. Chem. Soc.* **1997**, *119*, 2069−2078. (f) Mitzel, F.; Boudon, C.; Gisselbrecht, J. P.; Seiler, P.; Gross, M.; Diederich, F. *Helv. Chim. Acta* **2004**, *87*, 1130−1157. (g) Gisselbrecht, J. P.; Moonen, N. N. P.; Boudon, C.; Nielsen, M. B.; Diederich, F.; Gross, M. *Eur. J. Org. Chem.* **2004**, 2959−2972.

(4) (a) Knapton, D.; Rowan, S. J.; Weder, C. *Macromolecules* **2006**, *39*, 651−657. (b) Iyer, P. K.; Beck, J. B.; Weder, C.; Rowan, S. J. *Chem. Commun.* **2005**, 319−321.

(5) (a) Lavigne, J. J.; Anslyn, E. V. *Angew. Chem., Int. Ed.* **1999**, *38*, 3666−3669. (b) Wright, A. T.; Anslyn, E. V.; McDevitt, J. T. *J. Am. Chem. Soc.* **2005**, *127*, 17405−17411. (c) Rakow, N. A.; Suslick, K. S. *Nature* **2000**, *406*, 710−713. Suslick, K. S.; Rakow, N. A.; Sen, A. *Tetrahedron* **2004**, *60*, 11133−11138. (d) Albert, K. J.; Lewis, N. S.; Schauer, C. L.; Sotzing, G. A.; Stitzel, S. E.; Vaid, T. P.; Walt, D. R. *Chem. Rev.* **2000**, *100*, 2595−2626.

10.1021/ja061112e CCC: $33.50

fluorescence, quantum yields, and emissive lifetimes are observed upon the addition of protons or metal cations. The changes of the cruciforms' photophysics upon exposure to protons and to metal ions are comparable and suggest that binding of either species occurs at the same molecular loci. The observed photophysics can be explained by the position and the spatial arrangement of the frontier molecular orbitals (FMO) and their interaction with cations.

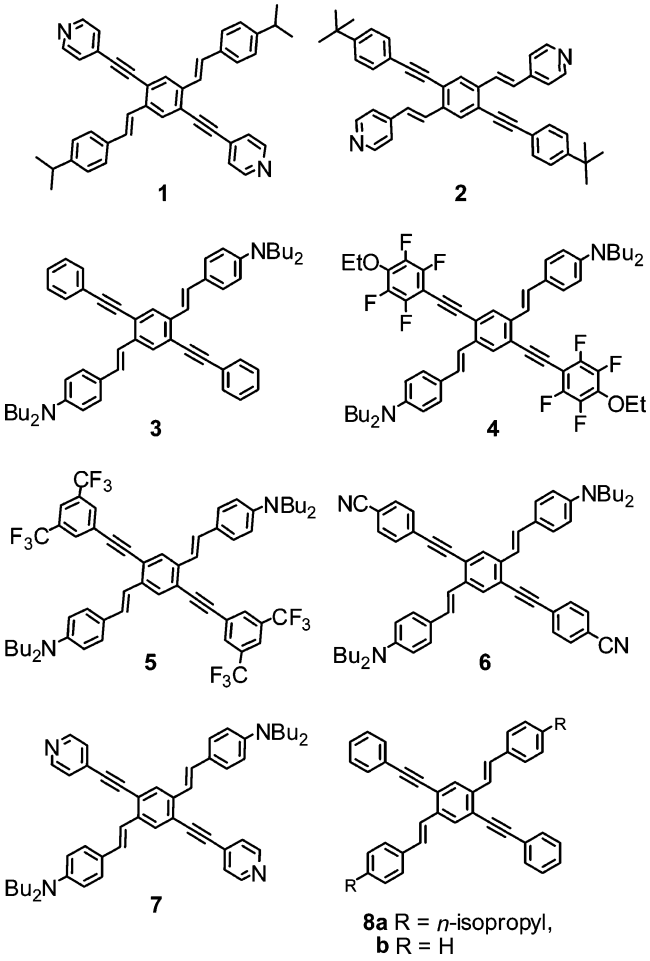

1,4-Distyrylbenzene was first synthesized in 1917 by Kaufmann through the reaction of benzylmagnesium bromide with terephthalic aldehyde followed by acid-catalyzed dehydration. Wittig, Horner, and Heck routes were developed subsequently.[6] The distyrylbenzene scaffold allows one to investigate changes in photophysical properties upon the attachment of donor and acceptor species.[7] Distyrylbenzenes find use as blue-emitting laser dyes and as model compounds for poly(*para*-phenylenevinylene)s (PPV) but are attractive chromophores in their own right with applications that range from fluorescence lifetime imaging to their use as cofactors in fluorescent antibodies.[8−11] If metal-complexing substituents are attached to the aromatic core, bis(aminostyryl)benzenes function as metal-sensing species, particularly if 15-crown[5] substituents are appended via an aniline nitrogen.[9] Significant blue-shift in the absorption is observed upon binding of various metal cations, but the emissive lifetimes remain almost unchanged.

Scheme 1. Synthesis of Cruciforms by a Combination of Horner and Sonogashira Methods

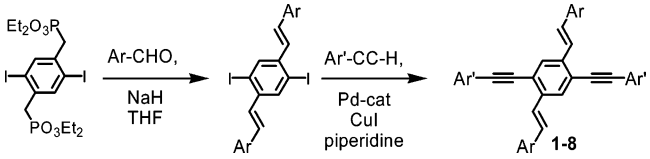

Similarly, bis(arylethynyl)benzenes were investigated as ligands for metal−organic networks and as model compounds for the respective conjugated polymers.[12] Their fluorescence lifetimes (table in the Supporting Information) (τ) range from $\tau = 0.32$ ns to $\tau = 2.5$ ns. Most of the emissive lifetimes are around $\tau = 1$ ns. The herein investigated cruciforms **1**−**8** are 1,4-distyrylbenzenes, yet their photophysical behavior and their spectroscopic responses to metal cations are significantly expanded.

Results and Discussion

Synthesis. Cruciform fluorophores[13−16] are π-systems in which two alkene and two alkyne arms are placed in a 1,4−2,5-relationship on a central benzene ring. The synthesis of cruciforms **1**−**3**, **5**, and **7** has been described in ref 13, while the synthesis of cruciforms **4**, **6**, and **8a** is presented in the Supporting Information. All of the cruciforms are made from a common precursor (Scheme 1); 2,5-bis(bromomethyl)-1,4-diiodobenzene is reacted with triethyl phosphite in an Arbuzov reaction. A Horner[17] olefination of the resulting bis(phosphonate)

(6) (a) Kaufmann, H. *Chem. Ber.* **1917**, *50*, 515−529. (b) Meier, H. *Angew. Chem., Int. Ed. Engl.* **1992**, *31*, 1399−1420. (c) Meier, H.; Lehmann, M. *Angew. Chem., Int. Ed.* **1998**, *37*, 643−645. (d) Meier, H.; Gerold, J.; Kolshorn, H.; Baumann, W.; Bletz, M. *Angew. Chem., Int. Ed.* **2002**, *41*, 292−295. (e) Deb, S. K.; Maddux, T. M.; Yu, L. P. *J. Am. Chem. Soc.* **1997**, *119*, 9079−9080. (f) Maddux, T. M.; Li, W. J.; Yu, L. P. *J. Am. Chem. Soc.* **1997**, *119*, 844−845. (g) Wang, S. J.; Oldham, W. J.; Hudack, R. A.; Bazan, G. C. *J. Am. Chem. Soc.* **2000**, *122*, 5695−5709. (h) Bazan, G. C.; Oldham, W. J.; Lachicotte, R. J.; Tretiak, S.; Chernyak, V.; Mukamel, S. *J. Am. Chem. Soc.* **1998**, *120*, 9188−9200. (i) Oldham, W. J.; Lachicotte, R. J.; Bazan, G. C. *J. Am. Chem. Soc.* **1998**, *120*, 2987−2988. (j) Scherf, U.; Müllen, K. *Synthesis* **1992**, 23−38. (k) Schenk, R.; Gregorius, H.; Meerholz, K.; Heinze, J.; Müllen, K. *J. Am. Chem. Soc.* **1991**, *113*, 2634−2647. (l) Scherf, U. *Top. Curr. Chem.* **1999**, *201*, 163−222.

(7) (a) Yang, J. S.; Chiou, S. Y.; Liau, K. L. *J. Am. Chem. Soc.* **2004**, *126*, 2518−2527. (b) Yang, J. S.; Liau, K. L.; Wang, C. M.; Hwang, C. Y. *J. Am. Chem. Soc.* **2004**, *126*, 12325−12335. (c) Yang, J. S.; Liau, K. L.; Tu, C. W.; Hwang, C. Y. *J. Phys. Chem. A* **2005**, *109*, 6450−6456. (d) Yang, J. S.; Lin, Y. D.; Chang, Y. H.; Wang, S. S. *J. Org. Chem.* **2005**, *70*, 6066−6073.

(8) Holzer, W.; Penzkofer, A.; Gong, S. H.; Bradley, D. D. C.; Long, X.; Bleyer, A. *Chem. Phys.* **1997**, *224*, 315−326.

(9) Barlow, S.; Risko, C.; Coropceanu, V.; Tucker, N. M.; Jones, S. C.; Levi, Z.; Khrustalev, V. N.; Antipin, M. Y.; Kinnibrugh, T. L.; Timofeeva, T.; Marder, S. R.; Bredas J. L. *Chem. Commun.* **2005**, 764−766.

(10) Matsushita, M.; Meijler, M. M.; Wirsching, P.; Lerner, R. A.; Janda, K. D. *Org. Lett.* **2005**, *7*, 4943−4946.

(11) (a) Bastiaens, P. I. H.; Squire, A. *Trends Cell Biol.* **1999**, *9*, 48−52. (b) Lakowicz, J. R.; Szmacinski, H.; Nowaczyk, K.; Berndt, K. W.; Johnson, M. *Anal. Biochem.* **1992**, *202*, 316−330. (c) Pepperkok, R.; Squire, A.; Geley, S.; Bastiaens P. I. H. *Curr. Biol.* **1999**, 9, 269−272. (d) Mayr, T.; Igel, C.; Liebsch, G.; Klimant, I.; Wolfbeis, O. S. *Anal. Chem.* **2003**, *75*, 4389−4396.

(12) (a) Evans, O. R.; Lin, W. B. *Acc. Chem. Res.* **2002**, *35*, 511−522. (b) Lin, W. B.; Evans, O. R.; Xiong, R. G.; Wang, Z. Y. *J. Am. Chem. Soc.* **1998**, *120*, 13272−13273.

(13) (a) Wilson, J. N.; Josowicz, M.; Wang, Y. Q.; Bunz, U. H. F. *Chem. Commun.* **2003**, 2962−2963. (b) Wilson, J. N.; Bunz, U. H. F. *J. Am. Chem. Soc.* **2005**, *127*, 4124−412. (c) Gerhardt, W. W.; Zucchero, A. J.; Wilson, J. N.; South, C. R.; Bunz, U. H. F.; Weck, M. *Chem. Commun.* **2006**, 2141−2143.

(14) (a) Marsden, J. A.; Miller, J. J. Shirtcliff, L. D.; Haley, M. M. *J. Am. Chem. Soc.* **2005**, *127*, 2464−2476. (b) Marsden, J. A.; Haley, M. M. *J. Org. Chem.* **2005**, *70*, 10213−10226. (c) Marsden, J. A.; Miller, J. J.; Haley, M. M. *Angew. Chem., Int. Ed.* **2004**, *43*, 1694−1697.

(15) (a) Hu, K.; Zhu, P. W.; Yu, Y.; Facchetti, A.; Marks, T. J. *J. Am. Chem. Soc.* **2004**, *126*, 15974−15975. (b) Niazimbetova, Z. I.; Christian, H. Y.; Bhandari, Y. J.; Beyer, F. L.; Galvin, M. E. *J. Phys. Chem. B* **2004**, *108*, 8673−8681.

(16) Klare, J. E.; Tulevski, G. S.; Sugo, K.; de Picciotto, A.; White, K. A.; Nuckolls, C. *J. Am. Chem. Soc.* **2003**, *125*, 6030−6031.

in THF as solvent with NaH as base affords 1,4-diiodo-2,5-distyrylbenzenes. The two aromatic iodides are substituted by alkyne modules in a Sonogashira−Hagihara coupling,[18] performed in piperidine with $(Ph_3P)_2PdCl_2$/CuI as catalyst system to give the cruciforms **1**−**7** and **8a** in good to excellent yields.

Spectroscopic Properties of the Cruciforms 1−7 in Dichloromethane. We have recently shown that **1**, **3**, and **7** are useful as fluorescent ligands for metal ions such as zinc, magnesium, and silver.[13b] Dual emission results if **7** is used as a ligand, because metal complexation can successively occur on the dibutylaniline and then on the pyridine units, or vice versa. The pyridine rings are the less basic ligands and only bind through the free nitrogen lone pairs. For the anilines, it is not readily apparent whether metal cations bind directly to the nitrogen or to the π-face of the electron-rich arene. We investigated the optical properties of cruciforms **1**−**7** and examined the change of their photophysical properties upon addition of either acid or an excess of zinc ions. Figures 1 and 3 and Tables 1−4 show selected spectroscopic data (absorption, emission, Stokes shift, radiative lifetime, quantum yields) for cruciforms **1**−**7** in solution and upon addition of either metal (Mg^{2+}, Ca^{2+}, Mn^{2+}, Zn^{2+}) triflates or upon protonation by trifluoroacetic acid. Figure 2 shows a photograph of solutions of **1**−**7** under a blacklight. The top row depicts the chromophores alone, while in the middle and bottom rows the same chromophores are presented after addition of trifluoroacetic acid and zinc ions, respectively. The color changes of the brightly fluorescent cruciforms are spectacular; we expect these functional chromophores to show a significant potential for array applications, when equipped with additional auxiliary appendages.[5]

The absorption and emission spectra and the radiative lifetimes of **1**−**3**, **5**, and **7** are discussed in detail. The optical properties of **4** and **6** are included in Tables 1−4 but are similar to those of **5** and do not warrant separate discussion. Absorption and emission spectra of **4** and **6** are included in the Supporting Information. Figure 1 shows the absorption and emission spectra of **1**−**3**, **5**, and **7** in dichloromethane and hexanes.

The absorption spectra of the either donor- or acceptor-substituted cruciforms **1** and **2** are similar in shape, possessing one main transition around 330 nm and a second one at higher wavelengths that appears as a shoulder. The donor and the donor−acceptor cruciforms **3**−**7** (discussed here are **3**, **5**, and **7**) show a prominent, broad absorption feature around 450 nm and a second one with an additional shoulder at lower wavelengths. The low-energy band is intense in **4**−**7** and is due to a charge-transfer interaction of the donor and the acceptor groups. The emission spectra of cruciforms **1**−**7** in dichloromethane are broad and featureless with emission maxima ranging from 444 to 590 nm. The strongly donor−acceptor-substituted cruciforms **4**−**7** show red-shifted emission (561−590 nm) when compared to that of **1**−**3** (444−519 nm). The quantum yield of **1**−**3** in halogenated solvents is in the range of 0.3−0.7, while the donor−acceptor-substituted cruciforms **4**−**7** display quantum yields that are lower and range from 0.05 to 0.11. The quantum yield is qualitatively inversely correlated with λ_{max} emission in these species—the lower energy the emission, the lower of the fluorescence quantum yield. The decrease of emission quantum yield upon red shift of the emission is not unexpected, as nonradiative pathways (vibronic coupling) are more accessible in compounds with a smaller band gap.[19] However, in **1**−**7**, there is no clean numerical correlation between band gap and emission quantum yields.

The normalized emission spectra of **1**−**7** and **8a** (in hexanes) are displayed in Figure 3. Their emissions appear blue-shifted in hexanes relative to those recorded in dichloromethane; their Stokes shifts are also smaller than the corresponding Stokes shifts in dichloromethane. The cruciforms **1**−**3** and **8a** show a vibronic progression ranging from 1097 to 1302 cm^{-1}, associated with the C═C-stretching mode of the distyrylbenzene arms. In these cruciforms, this numerical value is somewhat smaller than in simple aminostilbenes (1300 ± 80 cm^{-1}), probably due to increased conjugation.[6a] In **1**−**3**, the intensity of the main band is larger than the intensity of the vibronic progression while in **8a** both are of the same intensity. A classic interpretation would assert that the 0,0 transition is more prevalent than the 0,1 transition; concomitantly, in the excited state, the distortion around the stilbene double bonds would be only modest, because distortion correlates with an increased intensity of the vibronic progression. It is not clear if the classic picture holds for **1**−**3** and **8a**; their Stokes shifts are quite large and the main band might already be the vibronic 0,1 or 0,2 transition. Cruciforms **1**−**3** and **8** feature spatially delocalized HOMOs and LUMOs, and their emission spectra in hexanes are similar to those observed for stilbenes with analogous substituent patterns. Upon examination of the emission spectra of **4**−**7** in hexanes, one notices a bathochromic shift and a loss of vibronic fine structure. The more red-shifted the emission, the less vibronic fine structure is visible. For **4** and **7** there is still a shoulder, but in **5** and **6** this shoulder has largely disappeared. The increasing donor−acceptor character in **4**−**7** and the concomitantly increased internal charge-transfer character of the excited state makes it more distorted and explains the observed features (or the lack thereof). We hypothesize that the local separation of the FMOs in **4**−**7** is characterized by a loss of fine structure in their fluorescence spectra taken in nonpolar solvents—a convenient heuristic instrument to characterize novel cruciforms (vide infra).

If donor substituents are attached to the distyrylbenzene arms and acceptor substituents to the arylethynyl arms, the coefficient distribution of the FMOs changes. *The donor and acceptor substituents localize the FMOs on the respective arylethynyl and styryl branches*. The chromophores in these donor−acceptor-substituted cruciforms show a *disjoint* FMO structure. On the other hand, cruciforms devoid of the donor-acceptor pattern display FMOs that are spatially superimposable upon one another; we propose to call cruciforms with such an FMO arrangement *congruent*. The transition between congruent and disjoint is gradual but coincides with the occurrence of the intense charge transfer band that dominates their absorption spectra and the loss of fine structure in the emission spectra taken in nonpolar solvents. Organic chromophores with a disjoint FMO structure are quite rare but have recently been found in

(17) Horner, L.; Hoffmann, H.; Wippel, H. G.; Klahre, G. *Chem. Ber.* **1959**, *92*, 2499−2505.
(18) (a) Negishi, E.; Anastasia, L. *Chem. Rev.* **2003**, *103*, 1979−2017. (b) Sonogashira, K. *J. Organomet. Chem.* **2002**, *653*, 46−49. (c) Bunz, U. H. F. *Chem. Rev.* **2000**, *100*, 1605−1645.
(19) (a) Tolbert, L. M.; Nesselroth, S. M.; Netzel, T. L.; Raya, N.; Stapleton, M. *J. Phys. Chem.* **1992**, *96*, 4492−4496. (b) Englman, R.; Jortner, J. *Mol. Phys.* **1970**, *18*, 145−154. (c) Caspar, J. V.; Meyer, T. J. *J. Phys. Chem.* **1983**, *87*, 952−957.

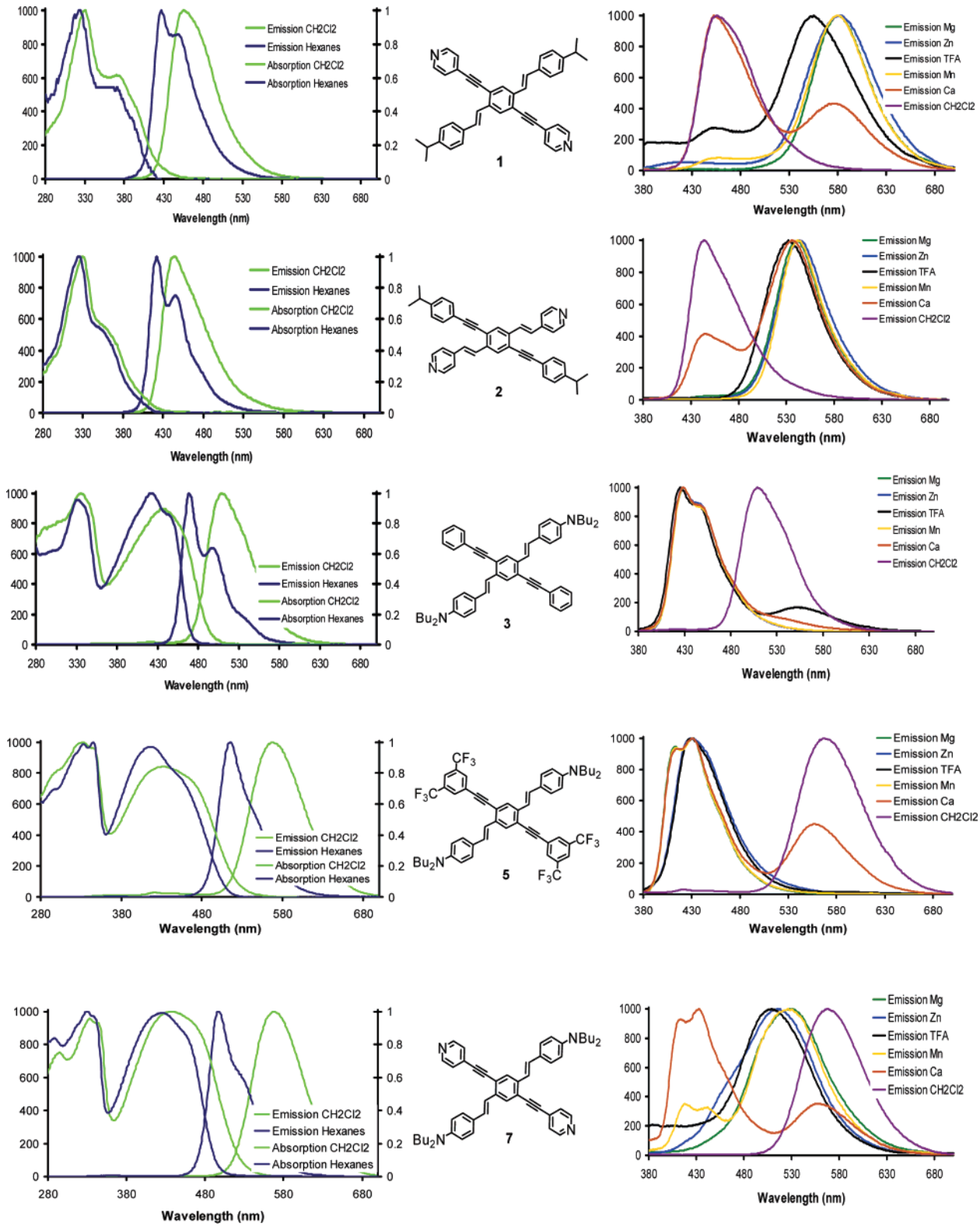

Figure 1. Normalized absorption and emission spectra of **1**−**3**, **5**, and **7**. Left: Absorption and emission spectra of **1**−**3**, **5**, and **7** in hexanes (blue) and dichloromethane (green). The emissions of **1**−**3** show vibronic spacing in hexanes. Right: Emission spectra of **1**−**3**, **5**, and **7** in dichloromethane (purple) and upon exposure to excess TFA (black), Mg^{2+} (green), Zn^{2+} (blue), Mn^{2+} (yellow), and Ca^{2+} (orange). The features in the emission spectra of **1** and **7** at 400−450 nm are due to artifacts from TFA. *y*-axis: arbitrary units of intensity.

diarylpyrazolines and were exploited by Fahrni et al. as sensory frameworks.[20] Generally, a disjoint FMO structure, i.e., spatially separated HOMO and LUMO, permits the independent tuning of the oxidation and reduction potential (or HOMO and LUMO) of such fluorophores. If one examines pars pro toto the disjoint FMOs of **7**, one notes that there is orbital overlap in the central benzene ring, but the overall overlap integral is not large; the HOMO−LUMO transition is symmetry-allowed and not de-

Table 1. Absorption and Emission Data for Cruciforms **1**−**7** and **8a** in Dichloromethane and Hexanes

cruciform	λ_{max} abs in CH_2Cl_2 (nm)	λ_{max} emission in CH_2Cl_2 (nm)	λ_{max} abs in hexanes (nm)	λ_{max} emission in hexanes (nm)	Stokes shift in CH_2Cl_2 (cm^{-1})	Stokes shift in hexanes (cm^{-1})	vibronic progressn (solvent) (cm^{-1})
1	330	456	324	427	5097	3978	1097 (hexanes)
	370		365	448	8373	7445	
	395 sh		390 sh				
2	330	444	325	422	5178	4632	1225 (hexanes)
	361 sh		353	445	7781	7073	
3	336	519	332	469	3668	2375	1242 (hexanes)
	436		422	498	10494	8799	
			447 sh				
4	337	561	334	509	4748	4277	
	352		348		10584	9089	
	443		418				
	479 sh		470 sh				
5	296	567	296	516	5458	4659	
	331		333		11099	9606	
	348		345				
	433		416				
	472 sh		461 sh				
6	340	590	321	514	6470	4641	
	361		344		10752	8714	
	427		355		12463	9615	
	478 sh		415				
			460				
7	295	567	288	496	5247	3368	
	333		330		11265	9164	
	346		341		12393	10142	
	437		425				
	472 sh		460 sh				
8a	331	419	327	409	2872	2650	1191 (CH_2Cl_2)
	374	441	369	432	6345	6131	1302 (hexanes)
	396 sh		390 sh				

Table 2. Emissive Data for Cruciforms **1**−**7** upon the Addition of Protons and Selected Metal Cations

cruciform	λ_{max} emission CH_2Cl_2 (nm)	λ_{max} emission with excess of H^+ (nm)	λ_{max} emission with excess of Zn^{2+} (nm)	λ_{max} emission with excess of Mg^{2+} (nm)	λ_{max} emission with excess of Mn^{2+} (nm)	λ_{max} emission with excess of Ca^{2+} (nm)
1	456	555	580	581	579	576
2	444	532	543	542	542	536
3	519	425	429	429	429	429
4	561	420	421	418	418	419
		438	440	440	422	440
5	567	430	429	413	414	417
				431	430	431
6	590	430	429	422	421	422
				432	435	432
7	567	509	518	530	418	414
					442	433
					526	560

Table 3. Quantum Yields of **1**−**7** upon the Addition of Protons and Selected Metal Cations

cruciform	quantum yield $CHCl_3$	quantum yield with excess of H^+	quantum yield with excess of Zn^{2+}	quantum yield with excess of Mg^{2+}	quantum yield with excess of Mn^{2+}	quantum yield with excess of Ca^{2+}
1	0.70	NA	0.31	0.49	0.46	NA[a]
2	0.67	0.06	0.18	0.28	0.22	NA[a]
3	0.31	0.44	0.62	0.79	0.69	0.76
4	0.15	0.65	0.80	0.85	0.86	NA[a]
5	0.09	0.68	0.84	0.94	0.89	NA[a]
6	0.05	0.38	0.58	0.86	0.79	NA[a]
7	0.11	0.06	0.11	0.23	NA	NA[a]

[a] NA: not available due to the presence of two emitting species in solution.

generate in the one-electron approximation. The disjoint FMOs explain the unusually long emissive lifetime as a consequence of this weakly Franck−Condon allowed transition. The large Stokes shifts in the disjoint cruciforms likewise support the assumption of a poor overlap of the ground with the excited state and corroborate the results obtained from the lifetime measurements.

Spectroscopic Data for Cruciforms 1−7 upon Addition of Trifluoroacetic Acid. If the FMO-localizing branches of the cruciforms contain free electron pairs such as in dialkylamino or pyridine units, the optical properties of such chromophores or luminophores should change upon metal ion complexation or protonation, directly shifting the HOMO or the LUMO positions. *That is observed in cruciforms* (Figures 1 and 2). To systematically explore this sensory response, the effect of protonation on the photophysics of **1**−**7** was examined. Upon

(20) Fahrni, C. J.; Yang L. C.; VanDerveer, D. G. *J. Am. Chem. Soc.* **2003**, *125*, 3799−3812.

Table 4. Radiative Lifetimes of **1**−**7** upon the Addition of Protons and Metal Cations[a]

cruciform	radiative lifetime τ (ns) $CHCl_3$	radiative lifetime τ (ns) with excess of H^+	radiative lifetime τ (ns) with excess of Zn^{2+}	radiative lifetime τ (ns) with excess of Mg^{2+}	radiative lifetime τ (ns) with excess of Mn^{2+}	radiative lifetime τ (ns) with excess of Ca^{2+}
1	4.1	3.7	3.9	5.0	4.9	3.4
	3.9	3.1	4.0			
	3.9	3.6				
2	3.8	6.7	6.8	6.9	7.0	6.4
		7.6	6.9			
3	1.7	2.6	3.1	3.0	2.9	2.8
		2.9	2.8			
4	4.2	3.5	3.1	2.9	2.8	2.7
	4.4	2.9	2.7			
		3.1	2.9			
5	4.4	2.8	2.6	2.9	2.9	2.7
	4.2	3.1	2.9			
6	3.9	2.5	3.7	3.4	3.0	2.9
	4.0	3.0	3.1			
		2.9	3.3			
7	4.3	1.8	2.1	2.1	1.3	2.6
	4.3	2.1	2.0			
		2.0				

[a] The lifetimes were monoexponential and fitted with a single decay function. In the case of Ca^{2+} the lifetime of the bound species was measured.

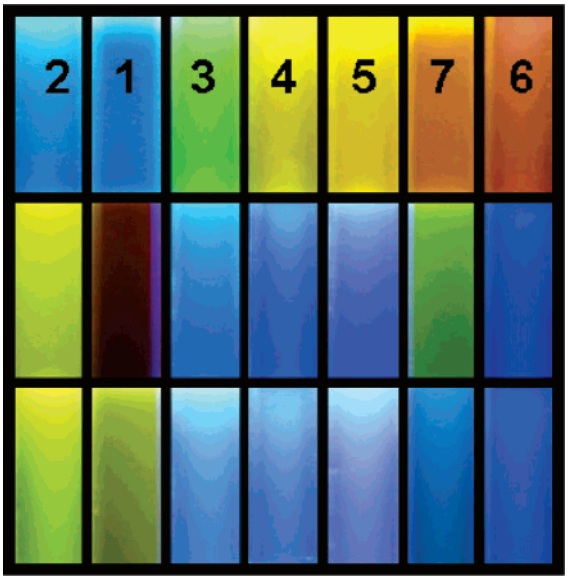

Figure 2. Emission of **1**−**7** in chloroform: (top) **1**−**7** without any additive; (middle) after addition of trifluoroacetic acid; (bottom) after addition of zinc triflate. The difference in the appearance of **7** and **1** in the presence of zinc triflate as compared to the pictures taken in the presence of trifluoractic acid is due to the inherent sensitivity profile of the used camera. All pictures were taken under a black light at a maximum emission wavelength of 365 nm.

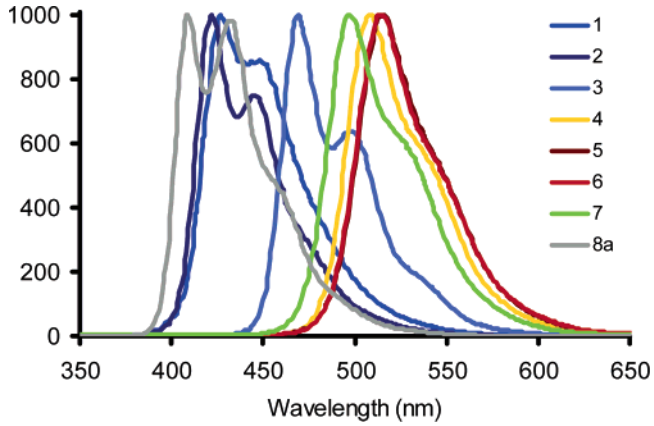

Figure 3. Emission of **1**−**7** and **8a** in hexanes. Emission maxima are presented in Table 1.

addition of an excess of trifluoroacetic acid (TFA) to the solutions of the cruciforms **1**−**7** in dichloromethane or chloroform, the absorptions of **1** and **2** experience a red shift, while the absorptions of **3**−**7** experience a significant blue shift (see absorption spectra included in the Supporting Information). These shifts are mirrored in the emission spectra of **1**−**7**, where upon protonation of **1** and **2** large red shifts are observed, while in **3**−**7** blue shifts occur. In **3** and **7** the effect is moderate; however, in **4**−**6** protonation results in a dramatic blue shift in excess of 150 nm. At the same time the fluorescence quantum yields change; in **1** and **2** the quantum yields drop from 0.7 to 0.06, while in **4**−**6** the quantum yields increase from 0.05−0.06 to 0.4−0.7 upon protonation. In the most extreme cases, **5** and **6**, the quantum yields increase by a factor of 7.5 upon protonation. Overall, there is a crude and qualitative correlation with the energy gap law.[19]

Upon protonation, cruciforms **1** and **2** show bathochromic shifts and **3**−**6** hypsochromic shifts, while **7** shows a blue shift followed by a red shift with decreasing the pH (Figure 5). The unusual response exhibited by **7** can be rationalized by qualitatively examining relative energies of the FMOs as the solution pH is decreased. The absorption and emission maxima in unprotonated **7** are well correlated with the relative HOMO and LUMO energies obtained from the ab initio calculations. The FMOs are disjoint (Figure 4), and binding of a positive ion to the aniline branch, where the HOMO resides, will lead to a stabilization of the HOMO but will leave the LUMO unchanged (Figure 6). The electronic transitions (absorption and emission) will be shifted toward shorter wavelengths. If a cation binds now to the pyridine moieties, the LUMO will be stabilized but the position of the HOMO will be barely influenced. As a consequence, the HOMO−LUMO gap will shrink and both absorption and emission will be red-shifted (Figure 6).

To investigate the effect of protonation on the spectra of **7** in more detail, we performed a titration in THF/methanol; **7** is attractive as it contains both pyridine and dibutylamino substitutents (Figure 5). Upon addition of acid, the emission of **7** (λ_{max}^{em} = 598 nm—note that, in THF/methanol, the emission of **7** is red-shifted when compared to the emission recorded in dichloromethane) diminishes and is replaced by an emission at 445 nm, corresponding to **7** with dibutylamino-protonated arms

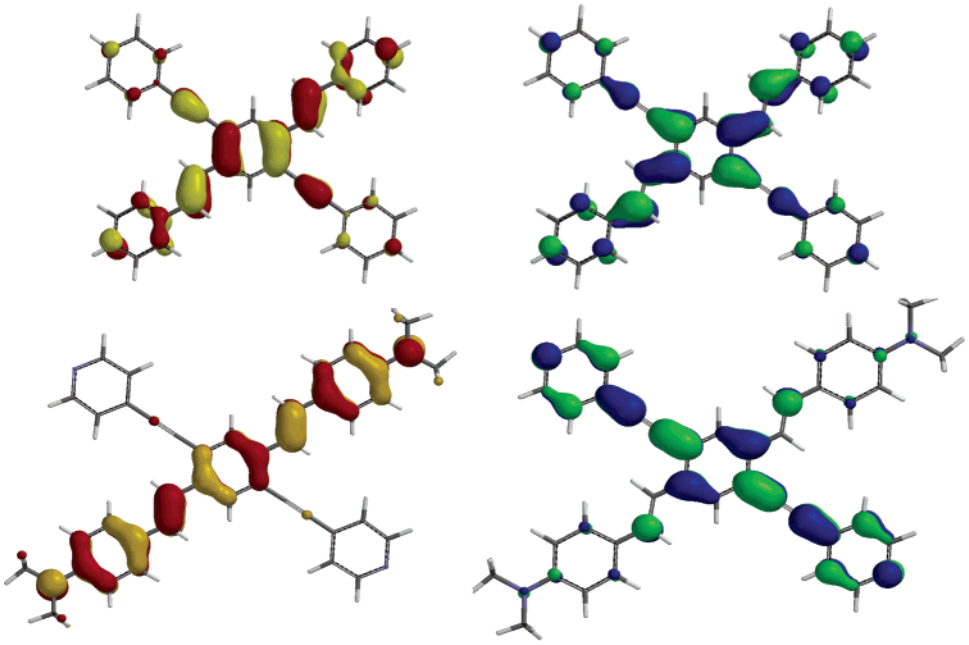

Figure 4. Top: Frontier molecular orbitals of **8b** calculated with B3LYP 6-31G**//6-31G** using Spartan. Left: HOMO (−5.17 eV) of **8b**. Right: LUMO (−2.00 eV) of **8b**. Bottom: Frontier orbitals of **7** calculated with B3LYP 6-31G**//6-31G** using Spartan. HOMO (−4.63 eV) (left) and LUMO (−2.07 eV) (right) are localized on the different branches of the molecule.

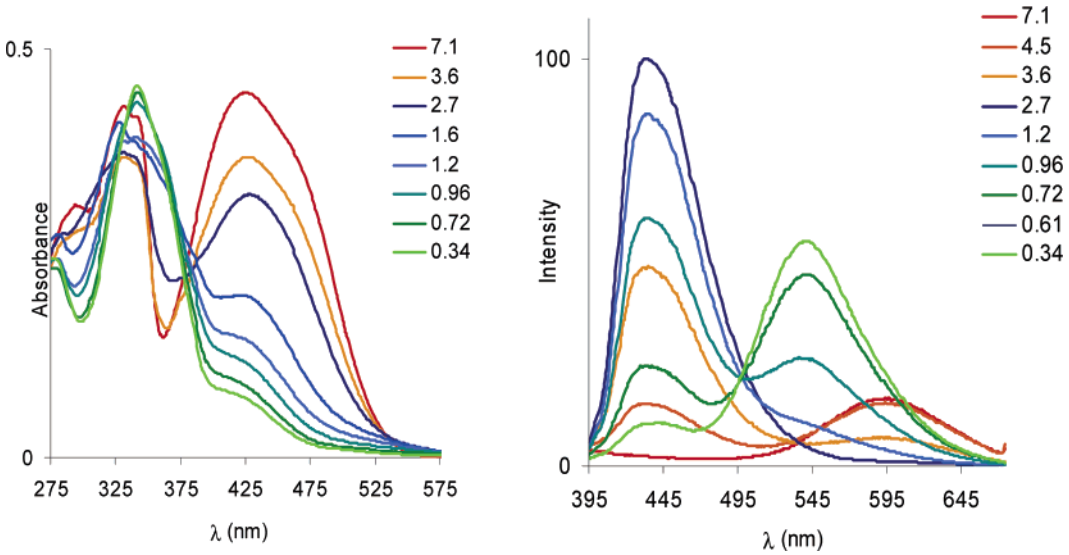

Figure 5. Protonation of **7** in methanol with trifluoroacetic acid. Emission maxima are 598 nm at pH 7.1, 437 nm at pH 2.7, and 542 nm at pH 0.34.

(λ_{max}^{em} = 445 nm). At pH 3.6, an approximate 1:1 ratio of the dibutylamino-protonated species (λ_{max}^{em} = 445 nm) and the nonprotonated species (cruciform **7**) is found. At a pH of 2.7 all of the nonprotonated **7** has disappeared, and only protonated species emitting at 445 nm are observed.[21] Diethylaniline has a pK_a of 6.67, while pyridine displays a pK_a of 5.25; from the pH-dependent optical data we conclude that (a) the dibutylamino group is protonated first and (b) both dibutylamino groups are protonated independently. *If that were not the case, i.e., if monoprotonation would happen, one would expect the disappearance of 50% of the neutral species to be complete at pH 6.6 and not at 3.6.*

Upon further protonation, a second isosbestic point is found and an emission centered at 542 nm grows in. We attribute this species to a cruciform **7** that is protonated at the dibutylamino arms *and* at the pyridine rings. From the above discussion we conclude that either one or both pyridine rings could be protonated, depending upon the difference in pK_a values of the monoprotonated pyridine and the diprotonated pyridine species. In the second case, the pK_a values of all four basic sites would be largely independent and successive double protonation of the dibutylamino and the pyridine group would occur.

To address the problem of the stoichiometry, we investigated the NMR spectra of **2** and **3**, in deuterated chloroform, and added TFA. Upon addition of TFA to either of the cruciforms we see only *one* set of sharp signals assigned to a symmetrical structure, suggesting in both cases that the respectively formed species is doubly protonated at the aniline or at the pyridine (Figures 7 and 8). In the case of a putative monoprotonated species, we would have expected to see a more complex and/or broadened NMR pattern. From the emission spectra of **1** and

(21) For a collection of pK_a values, see: http://www.zirchrom.com/organic.htm.

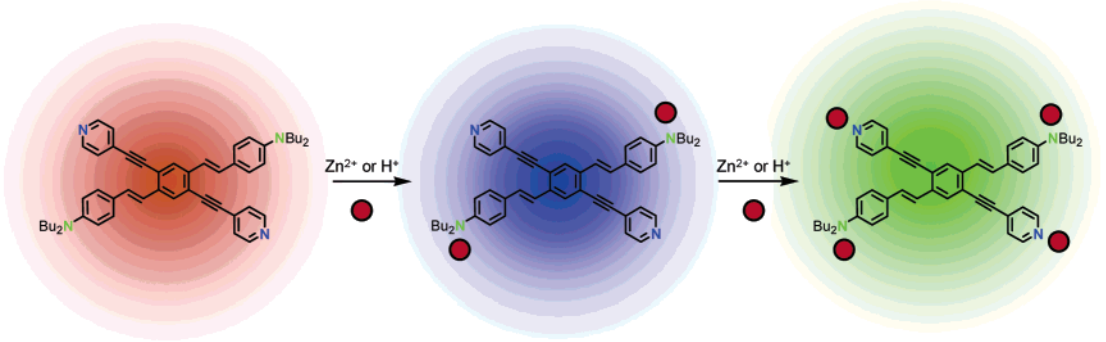

Figure 6. Sequential protonation or reaction of zinc ions with **7**.

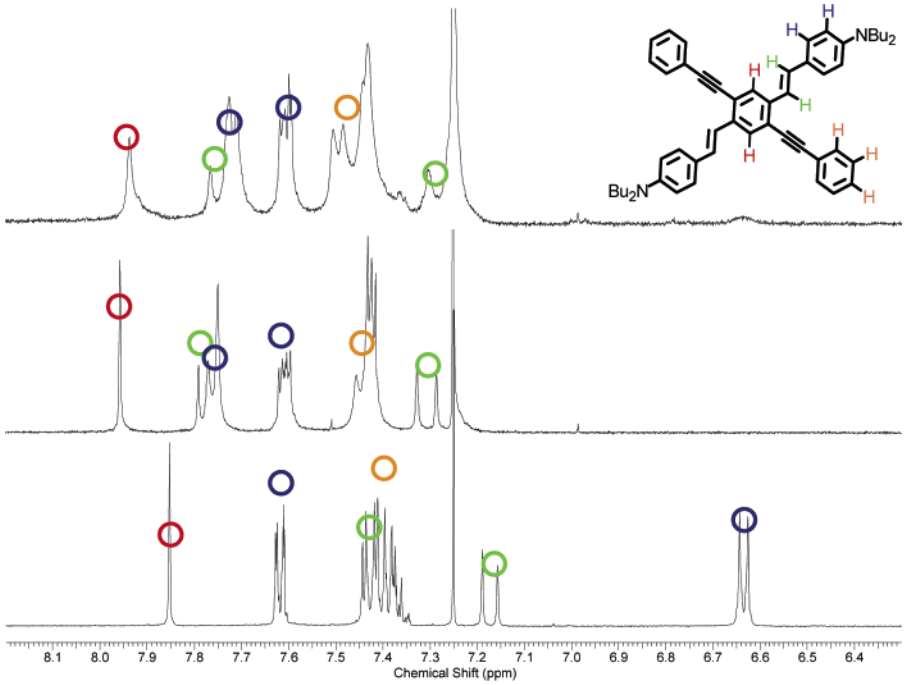

Figure 7. Proton NMR spectra of compound **3**: (top) after addition of an excess of zinc triflate; (niddle) after addtion of an excess of trifluoracetic acid; (bottom) **3** in chloroform-*d*. All spectra were taken at 500 MHz.

3 (Figure 1) we know that protonation produces one discrete species each, i.e., the NMR spectra taken under identical conditions cannot represent an equilibrium mixture of different protonated species. We conclude that in **7** we first doubly protonate the dibutylamino groups and then, in a second step, doubly protonate the pyridine units, suggesting that the pK_a values do not change much upon protonation of one end of the respective arm of the cruciform (Figure 6).

If one examines the fluorescence spectrum of **5** upon addition of trifluoroacetic acid in dichloromethane, there is a residual emission of the unprotonated species visible, suggesting that full protonation of the aniline sites is only achieved upon addition of a large excess of the acid. In **5** that is not too surprising, as the four CF_3 groups on the bis(phenylethynyl)-benzene branch *will* decrease the basicity of the dibutylaniline sites in a spillover process.

The change in radiative lifetime upon protonation varies from moderate for **5** (4.4 to 4.0 ns) to significant for **7** (4.4 to 1.8 ns). Both increase and decrease of the radiative lifetimes are found. The compound **2** shows an increase in lifetime from 3.8 to 7.2 ns upon protonation. These significant changes make the cruciforms potentially useful for fluorescence lifetime imaging (FLIM) applications.[11] In a broadly general sense, the emissive lifetimes increase upon decreasing the HOMO−LUMO gap and decreasing orbital overlap in the protonated species.

Addition of Zinc Triflate to Solutions of Cruciforms in Dichloromethane. The exposure of functional cruciforms toward zinc and other metal ions leads to chromic changes in absorption and emission.[13] It was of interest to examine more carefully the nature of the cation/cruciform interaction. More specifically, it was imperative to determine the locus of metal binding. In the case of the pyridines the binding site must be the lone electron pair. However, in case of cruciforms that contain dialkylaniline subunits, the metal cations could either bind to the electron-rich aromatic π-face or directly through the nitrogen of the dialkylamino group. Examples of metal cations binding to electron-rich aromatic π-faces are known; therefore, the question for the location of the metal cations is

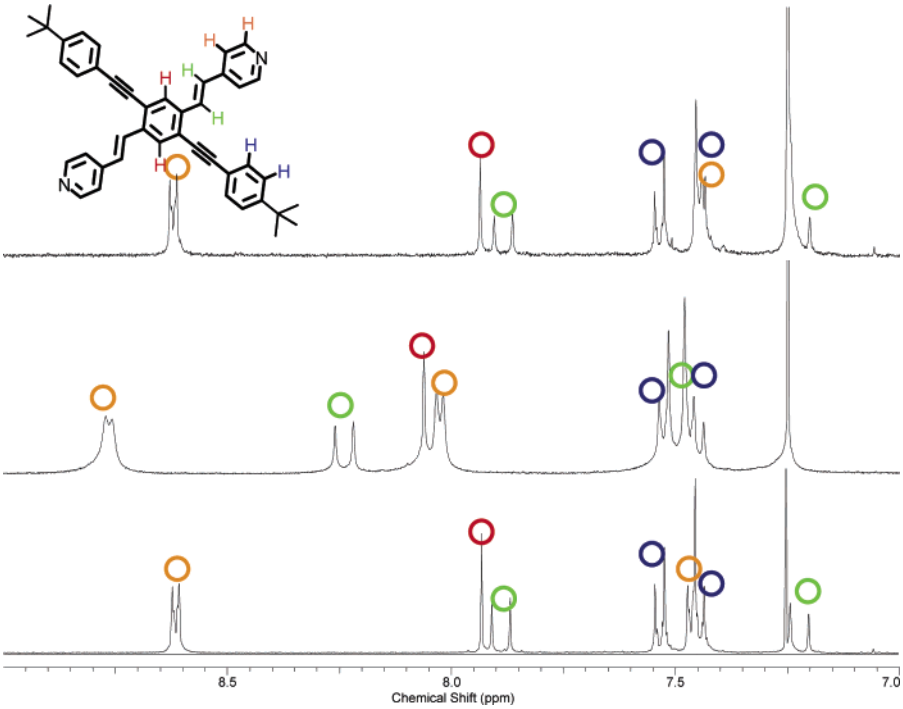

Figure 8. Proton NMR spectra of compound **2**: (top) after addition of an excess of zinc triflate; (middle) after addtion of an excess of trifluoracetic acid; (bottom) **2** in chloroform-*d*. All spectra were take at 400 MHz.

not trivial.[22] We selected zinc, a metal of importance in biology,[1,23] because it is in the d^{10} configuration and without optical transition in the visible.

How could one distinguish between zinc binding through the aniline nitrogens or through the electron-rich ring? In the reaction of cruciforms with TFA, the proton will bind to the free electron pair of the nitrogen; i.e., protonation will occur either at the pyridine-nitrogen or at the dibutylaniline. If the photophysical properties of the cruciforms upon exposure to protons and to zinc triflate are significantly different, one would conclude that zinc ions and protons would occupy different binding sites. Figures 1−3 and Tables 1−4 *show, however, that changes in spectroscopic properties, quantum yields, and emissive lifetimes of **1**−**7** are similar upon addition of zinc triflate and of TFA.* The discussion of the photophysical properties of **1**−**7** upon addition of TFA holds as well for the photophysics resulting from the addition of zinc salts. In both cases, the positive charge is the determining issue. Addition of zinc triflate to the pyridine-containing cruciforms leads to a somewhat larger red-shift in emission and to higher fluorescence quantum yields when compared to the values obtained for protonation of the cruciforms. These findings may indicate a stronger binding of the divalent zinc ions than of the protons to the pyridine units of the cruciforms. However, the overall similarities of the series of photophysical data, obtained for protonation vs exposure to zinc ions, suggests that the zinc ions bind directly through the aniline nitrogens. We investigated the ^{1}H NMR spectra of the model cruciforms **2** and **3** upon addition of zinc triflate and observe (Figures 7 and 8) results that are comparable to those we have obtained for the protonation of these cruciforms, suggesting again the similarity of the processes involved. Binding of the zinc through the electron-rich aromatic π-face does *not* seem to be important in solution, but in the solid state the situation could be different.

Fluorescence Response of Cruciforms to the Addition of the Triflates of Mg^{2+}, Ca^{2+}, and Mn^{2+}. With the effects of the addition of proton acids and zinc ions secured, we were curious if other metal cations in their +2 oxidation state would affect the fluorescence of the cruciforms differently. We chose Mg^{2+}, Ca^{2+}, and Mn^{2+}, all as their triflates as suitable representatives, because they are similar to zinc ions in their overall properties. Manganese and magnesium ions have roughly the same size as zinc ions, and only calcium is bigger (Zn^{2+} 88 pm, d^{10}; Mn^{2+} 89 pm, d^5; Mg^{2+} 86 pm, d^0; Ca^{2+} 114 pm, d^0).[24] The main difference is the increase in hardness when going from Zn^{2+} to Mg^{2+} and the presence of five unpaired electrons in Mn^{2+}. We were interested to see if the presence of the unpaired electrons would lead to a quenching of the fluorescence of the cruciforms and how increasing hardness and size would influence binding to the cruciforms. Figure 1 and Tables 2−4 show the pertinent results of the binding of all four metal cations to **1**−**7**. We will discuss the metal responses of the cruciforms **1**−**3**, **5**, and **7** in more detail. Upon exposure to the set of four metals, cruciforms **1**−**3** show large but metal independent shifts, similar to those obtained for zinc ions. In cruciform **2** the response is somewhat more varied with the emission maxima ranging from 536 to 543 nm upon addition of the metal cations. In **1** and **2**, the addition of Mg^{2+}, Mn^{2+}, and Zn^{2+} transforms all of the fluorophore into a metal-bound species, while in the case of Ca^{2+} only partial binding occurs.

(22) (a) Hirsch, K. A.; Wilson, S. R.; Moore, J. S. *Inorg. Chem.* **1997**, *36*, 2960−2968. (b) Venkataraman, D.; Lee, S.; Moore, J. S.; Zhang, P.; Hirsch, K. A.; Gardner, G. B.; Covey, A. C.; Prentice, C. L. *Chem. Mater.* **1996**, *8*, 2030−2040. (c) Hirsch, K. A.; Wilson, S. R.; Moore, J. S. *J. Am. Chem. Soc.* **1997**, *119*, 10401−10412.

(23) Suh, S. W.; Jensen, K. B.; Jensen, M. S.; Silva, D. S.; Kesslak, P. J.; Danscher, G.; Frederickson, C. J. *Brain Res.* **2000**, *852*, 274−278.

(24) Values from http://www.scescape.net/~woods/.

One can observe bound and unbound species. The more electron-rich **2** binds better to Ca^{2+} ions and the ratio of the emission intensity bound/unbound cruciform is considerably larger than in **1**.

Compound **5** with its strongly electron-withdrawing trifluoromethyl substituents shows a different response for Zn^{2+} than for Mg^{2+}, Mn^{2+}, and Ca^{2+}, as an additional blue-shifted feature is visible at 413−417 nm. The Zn^{2+}-induced emission is broad, featureless, and centered at 429 nm. Even saturated solutions of $Ca(OTf)_2$ leave a fraction of **5** unbound. The pyridine−dibutylamino cruciform **7** shows the most varied metal response. Both zinc and magnesium fully complex **7** but with different emission maxima (Zn^{2+}, 518 nm; Mg^{2+}, 530 nm). Manganese only binds partially to **7**. A feature at 418 nm is due to complexation of the dibutylamino groups while the second feature at 526 nm represents the fully, 4-fold-complexed **7**. In the case of Ca^{2+} we also see two different features. One corresponds to the uncomplexed cruciform, while the second one is observed at 414 nm and represents **7** in which only the two dibutylamino units are calcium-bound.

All of the cruciform−metal ion complexes are fluorescent. Their quantum yields are shown in Table 3. We were not able to determine the emission quantum yield of the Ca complexes, because we always (with exception of **3**) observe bound and unbound species. Generally, the Mg^{2+} complexes show the highest quantum yields, followed by the Mn^{2+} complexes. The Zn^{2+} complexes are the least fluorescent ones, only to be undercut by the protonated cruciforms. The reason for the metal-based variations in the fluorescence quantum yield is not clear, and it is not reflected (Table 4) by changes in the radiative lifetimes. Here all of the different metal complexes of one cruciform show similar fluorescence lifetimes.

From these results a self-consistent picture emerges. The cruciforms can be ordered in their metal binding power as **3** > **2** ≈ **5** ≈ **7** > **1**. The electron-releasing quality of the binding element seems to play the largest role. The metals can also be ranked in the power in which they bind the cruciforms, Mg^{2+} ≈ Zn^{2+} > Mn^{2+} > Ca^{2+}. The lesser binding ability of Ca^{2+} as compared to the other metal cations is due to its increased size and decreased charge density. Mg^{2+}, Zn^{2+}, and Mn^{2+} have all the same size and charge but are d^0, d^5, and d^{10} configured, respectively. Zn^{2+}, the softer metal ion, binds better to the pyridines than Mn^{2+}, which is expected. The second row ion, Mg^{2+}, the smallest and the hardest of all of the investigated ones, binds well both to the pyridine as well as to the dibutylamino groups. It was surprising for us that the d^5-configured Mn^{2+} did not lead to quenching of the fluorescence of any of the cruciforms, because we expected that unpaired electrons lead to spin−orbit coupling in the metal−cruciform complexes. Overall, the responses of the different metal cations to the different cruciforms are varied and the four cations can be discerned under ideal conditions. This is surprising, because the cruciforms were not designed to be metal sensory compounds.

Conclusions

The cruciforms **1**−**7** display radiative lifetimes considerably longer than those observed for distyrylbenzenes. The poor spatial orbital overlap of HOMO and LUMO in some cruciforms leads to a weakly Franck−Condon-allowed transition; the quantum yields correlate with the inverse of the emission wavelength. We have investigated the responses of spectroscopic properties of the cruciforms **1**−**7** to TFA and to the triflates of Mg^{2+}, Ca^{2+}, Mn^{2+}, and Zn^{2+}: In cruciforms the (dibutylamino)anilines are complexed first, because they are more basic than the pyridine sites, in accordance with pK_a values from literature sources.[21] Addition of protons or metal ions results in similar changes in the optical and NMR spectroscopic properties of all of the investigated cruciforms, suggesting that the metal ions and the protons bind to the same sites, viz. the free electron pairs of the dialkylaniline and the pyridine nitrogens. The parallel results observed for the addition of protons and metal ions suggests that protons can be used to qualitatively and conveniently assess the photophysical sensory responses observed in operationally functional fluorophores such as cruciforms, when positive charge is the major contributor to the change in fluorescence.[25]

In future contributions, we will report upon the binding constants of different cruciforms to Zn^{2+} and other metal cations and explore the use of water-soluble cruciforms in sensory applications. Suitable cruciforms will be recruited as members in sensor array libraries for the detection of metal cations. Last but not least, these functional chromophores show a wealth of unexpected photophysical properties that makes them attractive objects of study on their own.

Acknowledgment. We thank the National Science Foundation (Grants DMR 0138948, 2002−03, and DMR 0454471, 2004−05) and Georgia Institute of Technology for financial support, Prof. Laren Tolbert and Prof. Christoph Fahrni for helpful discussions, and Prof. Rob Dickson for the use of the CAROM lifetime spectroscopy setup. We thank Sandeep Patel for help with the lifetime measurements.

Supporting Information Available: Experimental details for the synthesis of cruciforms **4**, **6**, and **8a** as well as details for the photophysical experiments and the NMR experiments. This material is available free of charge via the Internet at http://pubs.acs.org.

JA061112E

(25) We thank an anonymous reviewer for this insight as well as the use of the term "operationally functional".